# METHODOLOGY FOR VALIDATION OF MATERIAL RESPONSE MODELS USING IN-SITU ABLATION SENSING METHODS

Colin Yee[1], Jon Langston[1], Hao Wu[2], and Joseph H. Koo[1,2*]

[1]The University of Texas at Austin, Dept. of Mechanical Engineering, Austin, TX 78712

[2]KAI, LLC, Austin, TX 78739

*jkoo@mail.utexas.edu

## ABSTRACT

A complete and efficient methodology for characterizing the pyrolysis response of ablative Thermal Protection Systems (TPS) materials is developed. The end goal of acquiring the inputs necessary for material response (MR) modeling in extreme hyperthermal environments is to permit rapid down-selection of TPS materials. The example case in this study focuses on the characterization of the MXB-360 glass/phenolic ablative for use in the Insulation Thermal Response and Ablation Code (ITRAC) developed by Northrop Grumman Innovation Systems. Aerothermal ablation testing was conducted on an oxyacetylene test bed with the use of small test models. Emphasis is placed on determining pyrolysis kinetic modeling constants by use of TGA, pyrolysis gas composition and enthalpy tables by energy dispersive x-ray (EDX) spectroscopy, and in-depth temperature profile matching by in-situ ablation sensing methods. Sensor construction methods, oxidizing versus non-oxidizing environment considerations, data analysis of in-situ ablation sensing methods, and validation criteria for MR modeling are briefly discussed.

## 1. INTRODUCTION

### 1.1 Background

Increased commercialization of space and renewed interest in hypersonic in-atmosphere flight has spurred the need for light weight, high-performance composite Thermal Protection Systems (TPS). TPS are critical in protecting components from heating during hypersonic flight or reentry in order to ensure reusability of the flight chassis or safe delivery of the payload [1]. Flight testing and post flight analysis is traditionally utilized to test TPS as it is the most reliable way to subject material samples to the combination of heat, vibration, and shock associated with hypersonic flight [2, 3], but ablation and heating models must be made more reliable in order to minimize expensive flight testing and lengthy design cycle times [4].

Low cost testing of small material samples greatly streamlines the down selection process of materials for TPS use. This testing typically involves the use of either heated plasma [5, 6] or oxyacetylene torches [7, 8] to apply high heat flux to the material sample. Ablation testbed operation still requires a significant time investment however, and access to high-temperature hypersonic wind tunnels is gated by both scheduling and cost. Repeat testing under differing conditions or high numbers of samples may still be costly, so the use of reliable numerical modeling to simulate alternate test conditions streamlines the TPS development cycle.

*Copyright 2020. Used by the Society of the Advancement of Material and Process Engineering with permission.*

The modeling of ablation phenomena is complicated due to the moving boundary conditions combined with mechanical erosion, thermochemical erosion, and changing density. Material Response (MR) modeling codes make use of thermal and mechanical material properties, as well as pyrolysis Kinetic Modeling Parameters (KMPs) in combination with the Arrhenius equation, in order to simulate the decay of materials in high temperature environments [9]. While it is common practice to mechanically and thermally characterize materials as they are produced, KMPs and other ablation specific characteristics, such as net gaseous outflow (B') tables, are generally not provided by manufacturers and must be determined by the end user. Common mechanical and thermal property characterization will not be covered. As such, this methodology is developed as a training introduction for those familiar with engineering materials but with limited experience in designing or testing pyrolyzing ablative materials.

The decay state of a material acts as a function by which material properties between the virgin material and charred material can be bridged. KMPs are typically determined via Thermogravimetric Analysis (TGA) in either an inert or oxidizing environment and then validated against experimental data. Depending on the complexity of the material, KMPs may be determined for each reaction step that occurs during decomposition, which is also dependent on the availability of reactants in the environment. Accurate KMPs and heats of formation are critical in modeling the ablation of TPS materials as they are the foundation of an accurate decay state function and determine the rate of energy consumption or release while the material is decomposing.

Figure 1 shows the dominant effects associated with the ablation of TPS materials. Heat input to the material comes primarily from frictional heating of air at hypersonic speeds as well as radiation and convection heat transfer from the resulting plasma sheath [4]. The material pyrolyzes as it is heated, releasing decomposition gases which mostly diffuse back through the lower density material near the ablation front. The gases may then flow through the char layer, providing further heat input to the material as they either ignite or radiate. The diffusion of pyrolysis gases additionally results in internal stresses throughout the TPS material.

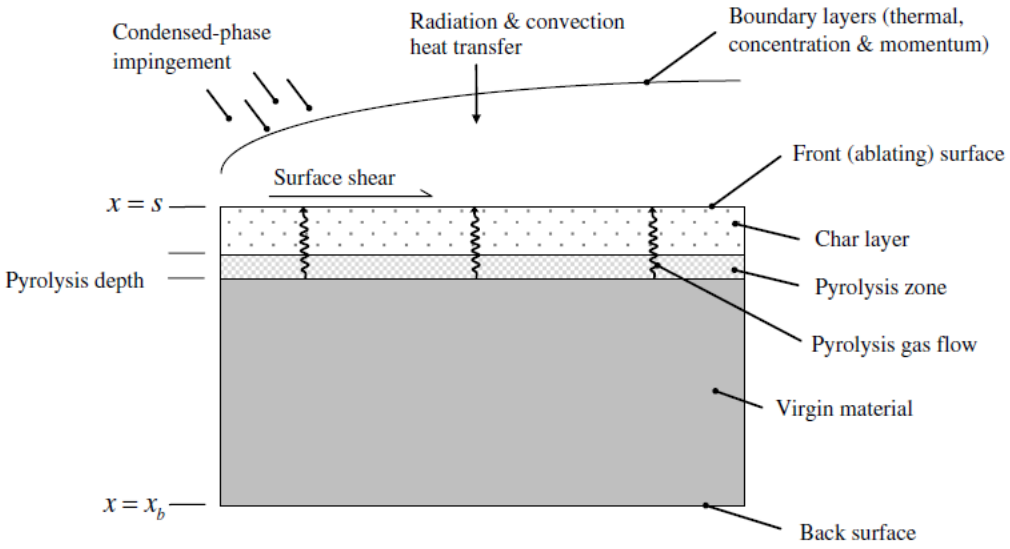


Figure 1. Ablation phenomena [10].

As the material continues to heat, the fully pyrolyzed char is removed by shear forces and the pyrolysis zone penetrates further into the virgin material. The virgin material and the back surface maintain a lower temperature than the ablating surface due to heat being removed by the heat of transformation, mass loss

through the removal of heated char, and mass loss through the diffusion of pyrolysis gases. Thus, structural and electrical components are maintained at a safe temperature while the ablating front is subjected to the extreme conditions of hypersonic travel through air. Predicting the expected mass loss of the shield, internal temperature gradient, and depth of ablation are critical for design engineers in order to ensure that the shielded components are adequately protected. Accurate simulation of TPS ablation reduces the time for iterative design. Additionally, high confidence MR modeling may permit a reduced safety factor and thus considerably reduce flight weight.

### 1.2 Arrhenius Equation

While heat and mass conservation equations can be utilized for fully virgin or char state material ablation, the density of a given section of material and its state of thermal decay are determined by the decay form of the Arrhenius reaction equation. The Arrhenius decay equation for change in extent of reaction with respect to temperature is described as follows:

$$\frac{d\alpha}{dT} = Ae^{-\frac{E_A}{RT}}f(\alpha) \quad [1]$$

Where α is the extent of reaction between virgin and char states, A is the Arrhenius pre-exponential, $E_A$ is the activation energy of the material, R is the universal gas constant, and f(α) is the reaction model function [9]. The extent of reaction α can be described as a ratio of the density difference of the material between the virgin and char states compared to the current density:

$$\alpha = \frac{\rho_v - \rho_s}{\rho_v - \rho_c} \quad [2]$$

With $\rho_v$ being the virgin density, $\rho_s$ being the current density, and $\rho_c$ being the char density. At a virgin state, $\rho_s$ is equal to $\rho_v$ and α is equal to zero; at a fully charred state, α is one. The changes in all material properties from the virgin to the charred material state are approximated by α, which acts as a linear interpolation term. The reaction model function can be described differently depending on what model is being utilized. Commonly, either the Friedman or Kissinger model are utilized: [11]

$$f(\alpha) = (1-\alpha)^n \alpha^m [-\ln(1-\alpha)]^P \quad [3]$$

$$f(\alpha) = (1-\alpha)^m \quad [4]$$

Where m, n, and p are experimentally determined curve fit parameters. Another method described by Ozawa [12] uses an arbitrary curve fitted to TGA data for the reaction model function f(α). KMPs as a whole refer to these reaction model function curve fit parameters (n, m, p, etc.) along with Arrhenius pre-exponential and the activation energy.

## 2. TEST METHODS

### 2.1 Thermogravimetric Analysis (TGA)

TGA is performed by weighing a sample of material inside an insulated furnace with a scale while its temperature is increased by a constant heating rate. The temperature is raised to a high temperature (typically in the range of 1,000 to 1,600 °C) and the sample is weighed at a fixed time interval. A purge gas, normally either air or nitrogen, is used to remove pyrolysis gases and ensure that only the solid material is

weighted. This permits the user to observe how the material degrades in increasingly high temperature environments while also separating the degradation reactions. It is also more expeditious than multiple material degradation tests at constant temperature and compensates for degradation that occurs during the heat up to a constant temperature test [12]. Structure changes in polymers at constant high temperatures also makes constant heating rate TGA the preferred method of determining KMPs.

The number of degradation reactions in a material undergoing TGA is normally observed by the number of inflection points in the mass versus temperature curve, pictured below in Figure 2. While polymer degradation is very complex, bulk KMP determination focuses on analyzing the dominant reaction chains as a combined group.

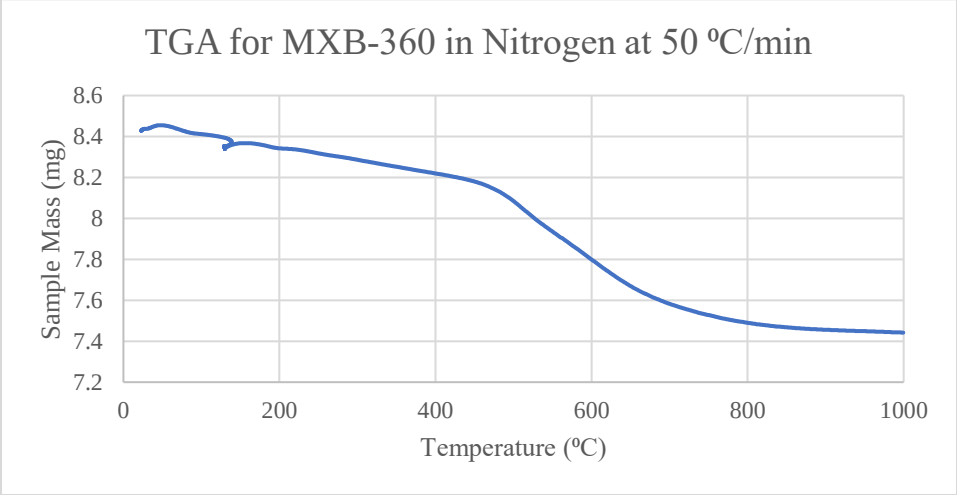


Figure 2. TGA data for MXB-360 glass/phenolic at a heating rate of 50 °C/min using nitrogen as a purge gas with a flow rate of 50 ml/min.

The TGA data in Figure 2 was generated using a TGA-50 from Shimadzu Scientific Instruments. The 10 mg MXB-360 samples were heated in either a nitrogen or air environment from room temperature to 130 °C and then maintained at that temperature for 30 minutes in order to remove any moisture. At the end of the drying period, the TGA-50 directly heats the sample at a constant heating rate up to 1,000 °C. The purge rate of the air or nitrogen is maintained at 50 ml/min in order to adequately remove pyrolysis gases while minimizing risk of disturbing the material sample in the furnace.

### 2.2 Aerothermal Heating Test Beds

For destructive testing of charring materials, aerothermal test beds provide low cost alternatives to heating during flight testing. Aerothermal test beds use heated gas flows to enable a combination of convective and radiative heat transfer to the test model. Common choices for aerothermal testing are oxyacetylene test beds (OTB) used to simulate oxidizing conditions (*i.e.*, solid rocket exhaust) [13] or inductively coupled plasma (ICP) torches shown in Figure 3 which can simulate non-oxidizing or less-oxidizing (*i.e.*, atmospheric reentry) environments with the use of inert gases.

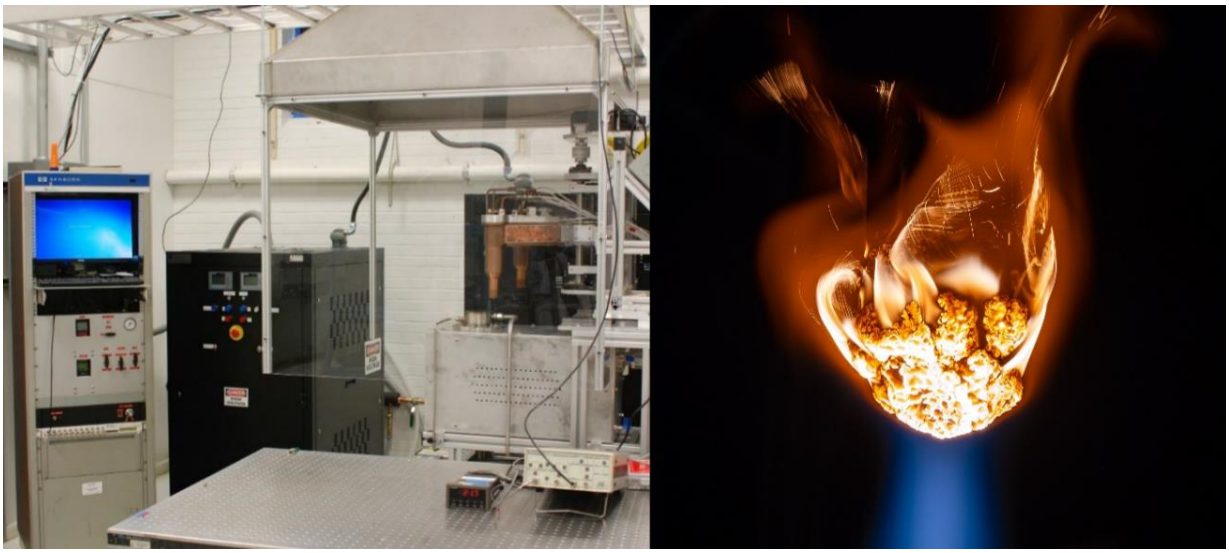

Figure 3. An ICP torch with robotic armature located at the University of Texas Pickle Research Campus (left). A thermoplastic test model undergoing testing in the ICP in an argon environment (right).

While the heat flux applied to the test model may be accurately measured by a Gardon gage, many MR codes require the separation of convective heat flux from radiative heat flux. Instead of extensive use of instrumentation, which may not be feasible, computational flow dynamics (CFD) analyses may be used to extract flow speed, film coefficients, recovery enthalpy, and any other necessary flow characteristics required by the MR code.

Aerothermal testing is advantageous in that it produces many measurables from a single test, such as surface temperature, back-side temperature, in-depth temperature, mass change, volume change, depth of ablation, ablation rate, and pyrolysis zone depth. Morphological and compositional changes in the charred and pyrolyzing material can be examined after testing.

It is important to select a test bed which closely represents the use conditions, as oxidizing flow can impact the temperature at which a material begins to decompose. For example, carbon fibers begin to decompose much sooner in an oxidizing flowfield than in a non-oxidizing flowfield; the result is that an oxidizing flow will cause a carbon fiber composite to char completely rather than delaminate, which will result in a significantly different internal and back-side temperature profile.

Figure 4. MXB-360 test model undergoing OTB aerothermal testing.

The in-situ ablation sensing data later presented for analysis was taken from a 30 mm diameter, 15 mm thick cylinder of MXB-360 glass/phenolic composite subjected to a 1,000 W/cm$^2$ heat flux for 60 seconds from the OTB pictured above in Figure 4. As OTB tests are inexpensive to construct and operate, and the test model used a minimal amount of material, as a result the cost of testing was minimized.

### 2.3 Energy Dispersive X-Ray (EDX) Spectroscopy

EDX utilizes the electron beam from a scanning electron microscope (SEM) to excite the electrons of the atoms of the observed material. As the electrons move back into a lower energy state shell, they emit X-rays, which are then counted by a sensor and sorted by energy. Different elements are then correlated to their signature x-ray energy and counts per electron volt, providing a quantitative elemental composition of the material.

While EDX is not able to measure lighter elements, such as hydrogen and nitrogen, it can be used to establish a base ratio and mass fraction for other elements. Ratios can then be used to determine light elements assuming there is not significant contamination by lighter elements, that the compounds in the material are relatively pure, and the general composition is known. Software can determine the accuracy of the counts, enabling EDX to give a rough elemental composition in a single low-cost step as opposed to using multiple mass spectrometry methods to obtain a complete elemental composition.

The EDX data used for surface thermochemistry simulation in this study was taken from a Hitachi S5500 STEM. Several samples of virgin MXB-360 were examined to establish an elemental composition baseline and identify contaminants present from the production process. Because the silica in MXB-360 separates from the phenolic during ablation, EDX spectroscopy was performed on the glass char and the carbonaceous char separately. Only the carbonaceous char was compared against the virgin material for the purposes of determining the pyrolysis gas composition, as it is assumed that the silica did not contribute significantly to the elemental composition of the gas, as discussed later.

## 3. ANALYSIS

### 3.1 In-Situ Temperature Sensing Data

Thermocouples embedded inside the material test model and on the backside are common methods of contact measurement during thermal ablation testing. Non-contact measurement is necessary for front-side temperature and can be achieved via IR pyrometer or IR camera. Based on front side, in-depth, back-side, and final heat-soaked temperature, the thermal state of the material can be well known throughout the duration of the test, providing a large amount of data for property determination and validation [13]. These temperature profiles can then be used to validate the MR model for the given material.

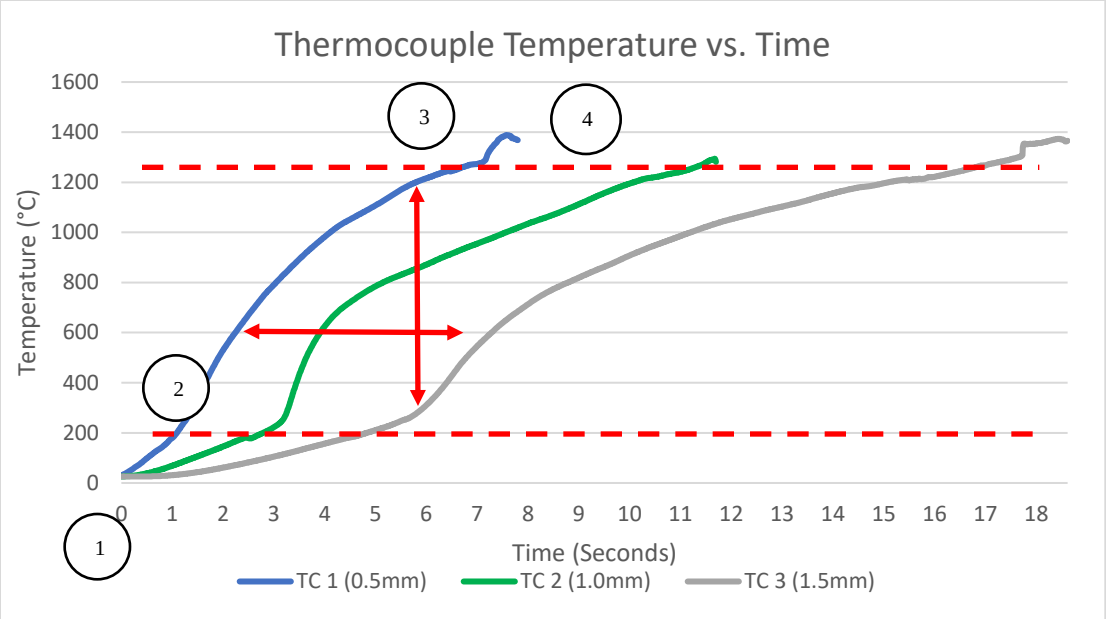


Figure 5. In-situ ablation sensing temperature data from three embedded thermocouples in an MXB-360 test model.

Figure 5 shows an example data set of three K-type thermocouples embedded at 0.5 mm, 1.0 mm, and 1.5 mm from the ablating surface of an MXB-360 glass/phenolic test model in an OTB calibrated to a heat flux of 1,000 W/cm$^2$. (1) Initial heating of the material occurs along with one minor reaction. (2) Between the dotted red lines, pyrolysis is ongoing for a single dominating reaction chain and a minor secondary reaction, resulting in a decrease in heating rate as the reactions consumes energy. At higher temperatures the reaction rate increases, consuming more energy and damping the heating rate further. Peak temperature difference (vertical red arrow) and ablation rate (horizontal red arrow) are simple to extrapolate from the curves. (3) The material has completely transformed to char and the last pyrolysis reaction no longer damps the heating rate. (4) The thermocouple extends out of the char layer as it erodes, and the thermocouple is destroyed by the front side heat flux.

Inflection points in heating can be used to help gage the number of reactions ongoing in the material during pyrolysis in the environment simulated by the test bed. Care should be taken not to disregard minor reactions, however, which will generally not appear as inflection points but will still influence the overall heating rate.

### 3.2 Mass Spectrometry for Pyrolysis Gas Enthalpy and Composition

Radiation and convection heating from the mixture of environmental gases and pyrolysis gases escaping the charring ablative material constitutes a significant amount of heat and mass transfer at the surface. In a subsonic flow field, convection will generally dominate as the primary mode of heat transfer, but radiation from gases at a bow shock boundary will dominate at higher Mach numbers. In order to adequately model the heat and mass transfer conditions at the boundary, the composition of the pyrolysis gas resulting from decomposition of the material must be well modeled. Net gaseous outflow ($B'$) must be tabulated as a function of pyrolysis gas ($B'_g$) and char consumption ($B'_c$) for a given material through thermochemical B-prime tables and T-chem tables. These tables may be generated from a surface thermochemistry program, such as Aerothermal Chemical Equilibrium (ACE) program, but only after the elemental composition of the pyrolysis gas and char are roughly understood [10].

Pyrolysis gas evolution at lower temperatures can be captured and analyzed through TGA/gas chromatography instrumentation. However, determining properties of pyrolysis gas evolved at very high heat fluxes is problematic. Pyrolysis gases in extreme hyperthermal environments will have differing compositions due to the amount of heat available and the potentially oxidizing environment; additionally, they immediately undergo further decomposition reactions and mix with the test bed flow gases upon escaping out of the front side of the material and then travel into the hot flow. Direct measurement would be extremely difficult, so a simpler method is to determine the pyrolysis products by simulating the decomposition of the mass fraction undergoing reaction to char.

Simulating pyrolysis gas formation at high temperature requires mass conservation, quantitative mass spectrometry, and a validated surface thermochemistry simulation code. The elemental composition differences between the virgin and charred state of the material are taken and the compared against mass fraction data from TGA. The reacting materials are fed into a reaction analysis code which can output the mixed pyrolysis gas enthalpies along with the chemical species that compose the pyrolysis gas. These enthalpy tables and gas composition tables are then utilized along with the elemental composition to determine thermodynamic properties and the equilibrium conditions at the surface at each step of the MR model [14].

If a high level of compositional fidelity is required, combinations of mass spectrometry methods can be combined in order to develop a detailed molecular and elemental composition. For example, combining carbon, hydrogen, nitrogen (CHN) analysis with a CHN analyzer; inductively coupled plasma-optical emission spectroscopy (ICP/OES) to determine trace metals; and ion chromatography (IC) to determine chlorine and sulfur content would yield a complete quantitative atomic composition. If basic assumptions about hydrogen content and lighter elements are permissible, single step methods, such as energy-dispersive X-ray (EDX) spectroscopy shown in Figure 6 may be utilized to save time.

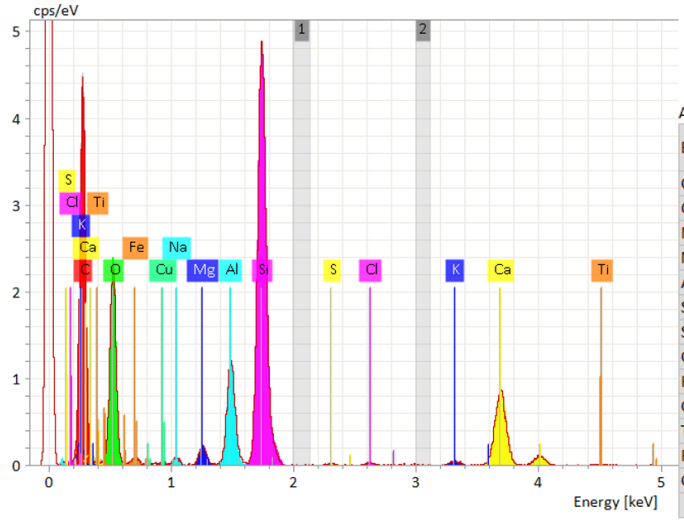


Acquisition

| Element | At. No. | Mass [%] | Mass Norm. [%] | Atom [%] | abs. error [%] (3 sigma) | rel. error [%] (3 sigma) |
|---|---|---|---|---|---|---|
| C | 6 | 64.48 | 48.87 | 61.01 | 22.43 | 34.78 |
| O | 8 | 41.24 | 31.26 | 29.29 | 14.86 | 36.03 |
| Na | 11 | 0.57 | 0.43 | 0.28 | 0.19 | 34.20 |
| Mg | 12 | 0.74 | 0.56 | 0.35 | 0.20 | 27.28 |
| Al | 13 | 3.47 | 2.63 | 1.46 | 0.57 | 16.28 |
| Si | 14 | 14.14 | 10.72 | 5.72 | 1.84 | 13.03 |
| S | 16 | 0.07 | 0.05 | 0.03 | 0.09 | 121.25 |
| Cl | 17 | 0.11 | 0.09 | 0.04 | 0.09 | 81.65 |
| K | 19 | 0.20 | 0.15 | 0.06 | 0.10 | 50.63 |
| Ca | 20 | 4.53 | 3.43 | 1.28 | 0.49 | 10.78 |
| Ti | 22 | 0.07 | 0.05 | 0.02 | 0.09 | 131.30 |
| Fe | 26 | 2.17 | 1.64 | 0.44 | 0.29 | 13.26 |
| Cu | 29 | 0.14 | 0.10 | 0.02 | 0.11 | 80.24 |
| | | **131.92** | **100.00** | **100.00** | | |

Figure 6. Two example read-outs from Energy-dispersive X-ray (EDX) spectroscopy of a glass/phenolic compound on a Hitachi S5500 STEM. Left: A graph of the X-ray peaks sorted by energy and tagged at the top with the most likely source element. Right: A chart showing the calculated elemental composition generated automatically by EDX software.

Once elemental composition differences between virgin and char materials are obtained, they may be combined with density properties and the mass fraction data from burn or TGA tests, then input into a

chemical equilibrium code. The resultant B' and T-chem tables may then be formatted for use by the desired MR model and serves as the primary form of surface thermochemistry and mass transfer reference for a material.

### 3.3 Kinetic Modeling Parameter (KMP) Development

Mass versus temperature data from constant heating rate TGA testing can be normalized to provide both percent mass loss and extent of reaction versus time. By rearranging the Arrhenius decay equation and the reaction model function, the KMPs for each decay reaction can be backed out and utilized to predict decay behavior in differing heating conditions, though the KMPs and decay reactions will change for differing environmental oxidative conditions. As the environment is assumed to have a fixed composition for these calculations, the decay reaction is not a function of environmental conditions, and thus KMPs would need to be derived for each expected environment that the material would be exposed to.

$$\frac{d\alpha}{dT} = Ae^{-\frac{E_A}{RT}}f(\alpha) \quad [1]$$

$$f(\alpha) = (1-\alpha)^m \quad [4]$$

For the remaining analysis, the single reaction order parameter form is used as given by Kissinger in equation (4). Utilizing the Kissinger equation instead of the Friedman equation will result in singular activation energy ($E_A$) and reaction order (m) values while the pre-exponential (A) will change dependent on the heating rate. While the Kissinger decomposition equation may not provide adequate simulation data above α values of 0.7, it is significantly simpler to numerically optimize the KMPs and is less computationally intensive than the Friedman method [11].

As the pre-exponential changes with heating rate for the Kissinger method, we can change the form of (1) in order to get another form of the Arrhenius equation:

$$\frac{d\alpha}{dT} = \frac{A}{\beta}e^{-\frac{E_A}{RT}}f(\alpha) \quad [5]$$

With β representing the heating rate dT/dt. We then further rearrange equation (5) such that:

$$\ln\left[\beta\frac{\frac{d\alpha}{dt}}{f(\alpha)}\right] = -\frac{E_A}{RT} + \ln A \quad [6]$$

$E_A$ and A can be extracted from a linear curve fit of the left side of equation (6) against 1/T based on TGA data. For this example, TGA data is taken from MXB-360 glass/phenolic compound with heating rates of 50, 20, and 10 °C/min using air as a purge gas, providing an oxidative environment. Commercially available TGA instruments typically are not capable of exceeding heating rates of 100 °C/min due to difficulty in construction and low demand for very high heating rates in the biomedical and industrial polymer fields. The first heating rate of 50 °C/min was chosen to be as high as the given TGA instrument can safely handle, while subsequent heating rates are approximately half as much as the previous in order to ensure significant separation on a logarithmic scale. While these heating rates are not representative of the approximately 200 °C/sec peak heating rate experienced during OTB testing, the use of three or more TGA data sets from differing heating rates can be used to predict realistic KMPs for all heating rates as demonstrated by Sihn

et al. [11] The temperature versus normalized mass loss graph in an oxidizing environment is shown below in Figure 7.

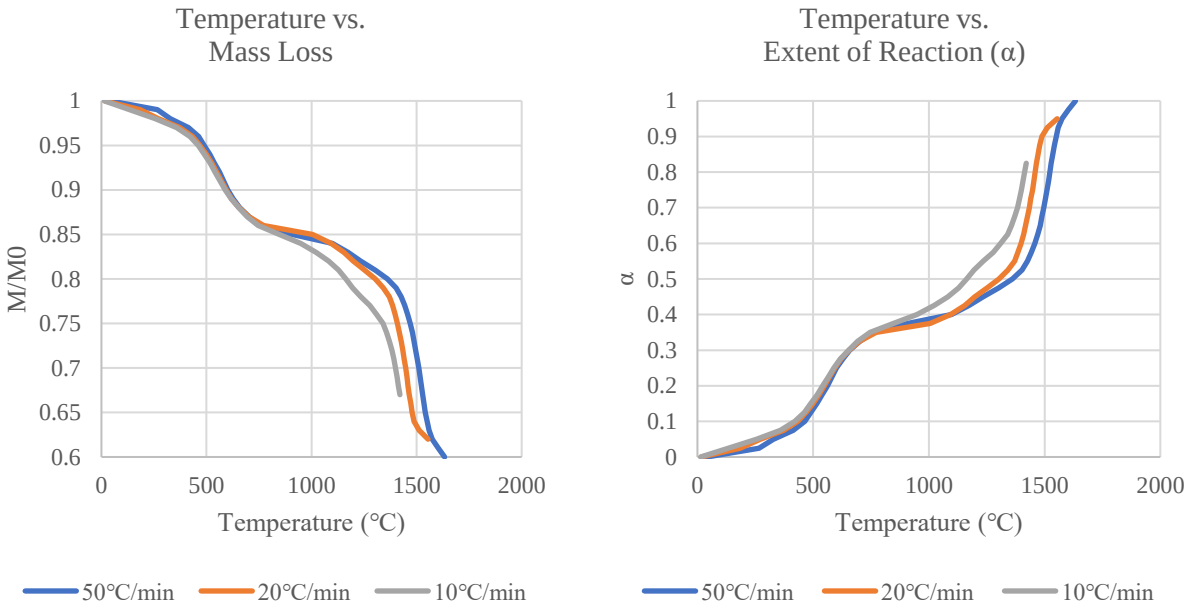


Figure 7. Left: TGA temperature versus normalized mass loss. Right: TGA temperature versus extent of reaction. Note that only two curves are immediately apparent in the data, one below 1,000 °C and one above.

By normalizing the data based on the initial and final mass fractions using equation (7), we can also develop the temperature versus overall extent of reaction (α) graph from Figure 7.

$$\alpha = \frac{M_0 - M}{M_0 - M_f} \qquad [7]$$

Where $M_0$ is the initial mass fraction, $M_f$ is the final mass fraction, and M is the mass fraction as a function of temperature. Equation 7 is also used to describe the extent of reaction for individual decomposition reactions ongoing in the material based on the mass fractions at which they initiate and terminate.

Based on these two graphs there are two distinct reaction regimes within the material, one below 1,000 °C and one above 1,000 °C. By determining the derivative of α with respect to temperature, the individual reactions can be observed directly. Three reactions take place, the first of which peaks at about 550 °C, the second at 1,200 °C, and the third at 1,450 °C. Figure 8 shows the combined and separated dα/dT data sets.

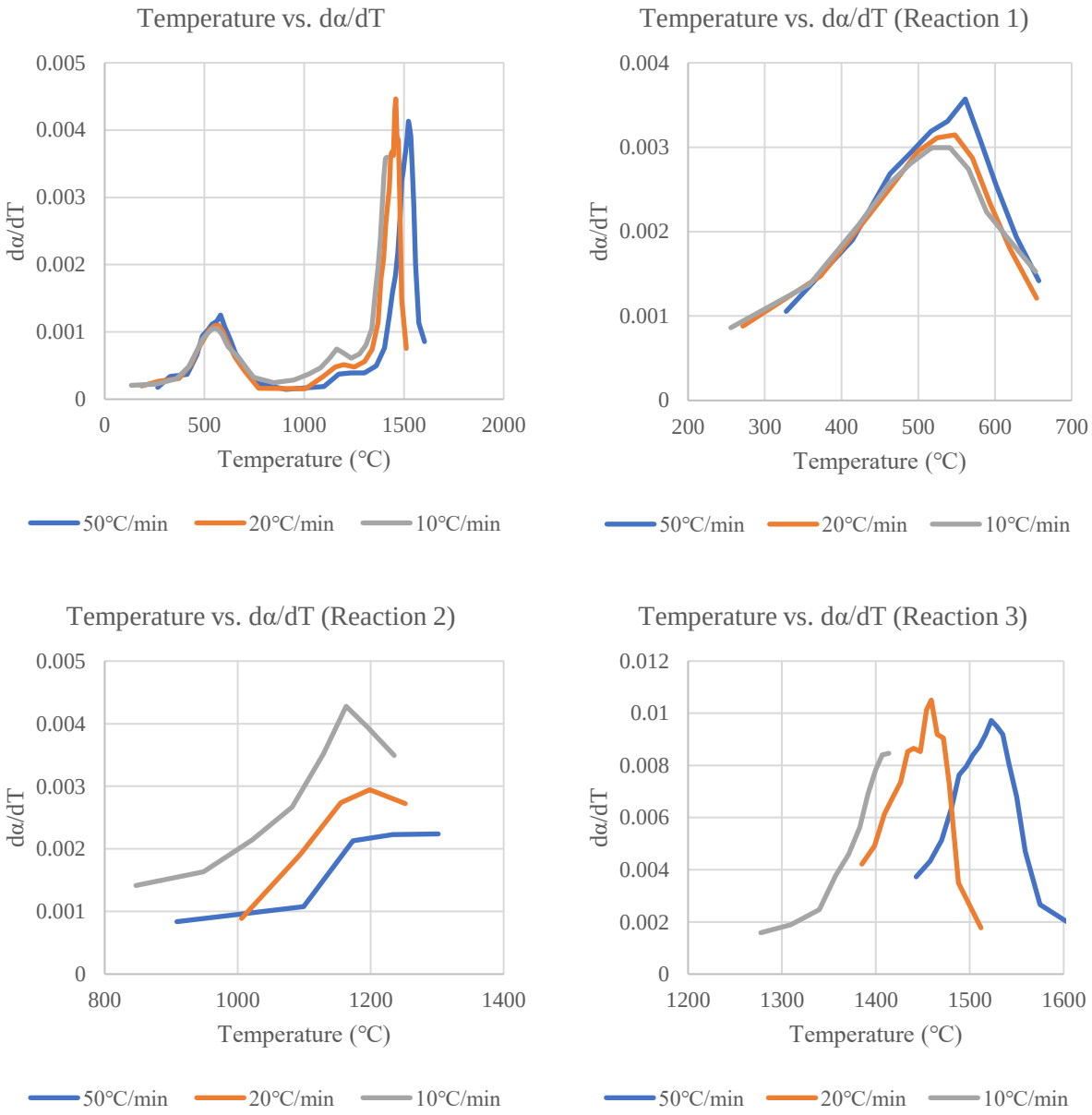


Figure 8. The combined temperature versus dα/dT curve for the MXB-360 TGA data and the individual temperature versus dα/dT curves for reactions one, two, and three.

With the β values known, only the value of f(α) is needed in order to determine values for the left side of (6). Using numerical methods, f(α) can be chosen to linearize the curves as much as possible as shown in Figure 9. Note that because of the decision to utilize the Kissinger equation (4) vice the Friedman equation (3) for f(α), the resultant curve will not reduce to a completely linear solution because the reactions overlap and the results fit better to a spline curve with more degrees of freedom. This will produce more error in activation energy $E_A$ and pre-exponential factor A while trying to determine the reaction order parameter *m*.

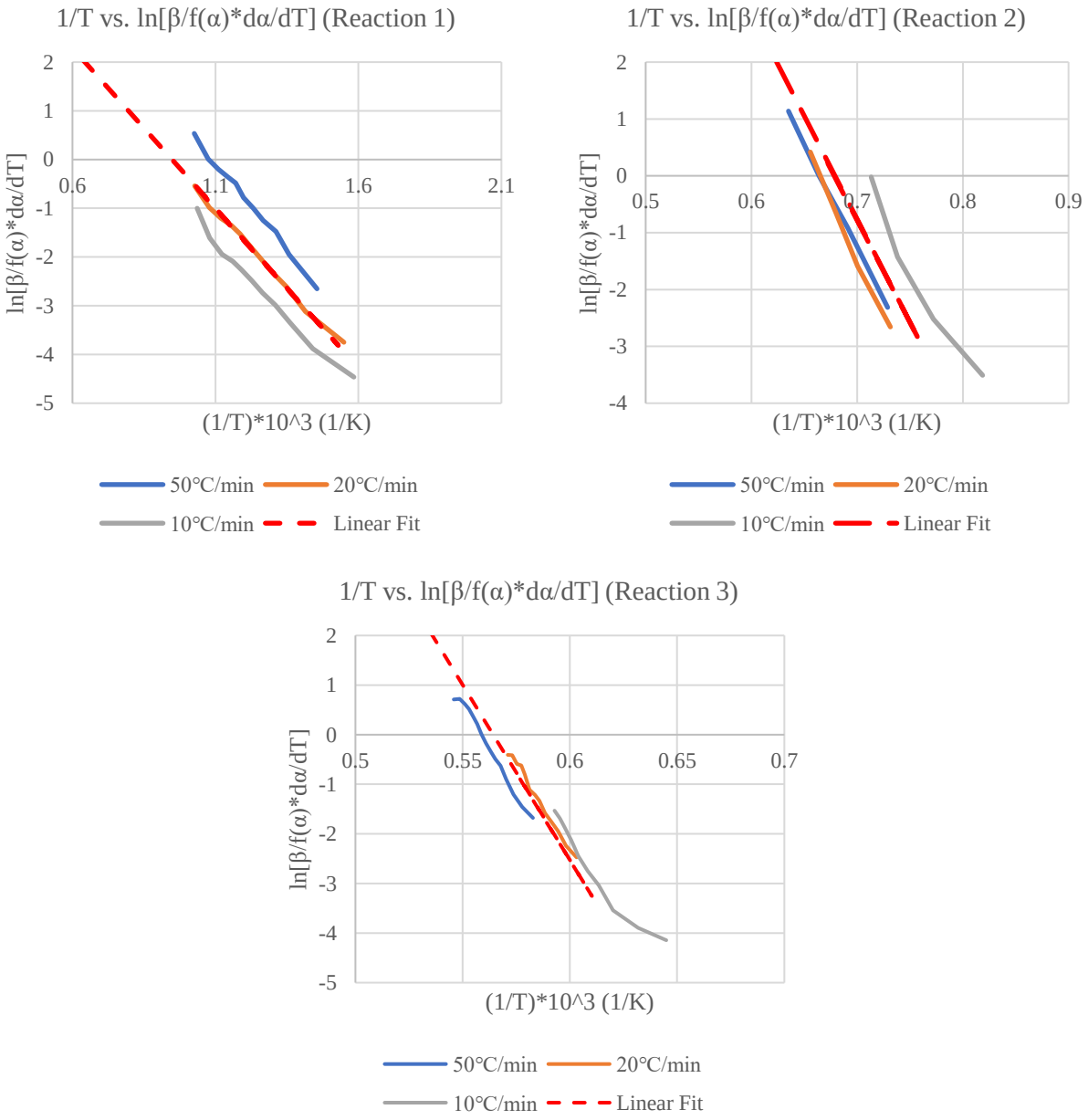


Figure 9. 1/T versus ln[β/f(α)*dα/dT] for reactions one, two, and three. A linear curve fit is performed on the average of the three curves for each reaction, generating the red dotted line, whose intercept is logarithmically proportional to the pre-exponential term and whose slope is proportional to the activation energy.

A least squares linear curve is separately fit to the data for each of the reactions. These fits are averaged together to generate the activation energy and pre-exponential term. In order to linearize the data as much as possible, the reaction order term *m* from equation (4) is varied in order to minimize the sum of the squares of Y-axis error from points on the fitted curves to points derived from data. This rudimentary method is fast and simple to implement using default tools provided with Microsoft Excel, though any number of numerical optimization methods may be employed to determine a reaction order term that best linearizes the data, and thus, is closest as possible to the best value for modeling the material. The individual reactions

may then be assigned mass fractions according to the data shown in Figure 8 and then validated by using an MR model and comparing the output against ablation test temperature data.

Table 1. KMPs for the three decomposition reaction chains based on the TGA data in an oxidative environment and the Kissinger method

| Reaction | 1 | 2 | 3 |
|---|---|---|---|
| m (unitless) | 1.205 | 3.927 | 1.244 |
| $E_A$ (kJ/mol) | 54.6 | 301.9 | 587.2 |
| A (1/sec) | $5.04x10^2$ | $5.02x10^{10}$ | $2.02x10^{17}$ |

With the reaction order term for f(α) fixed, the slope of the curve fit (1/RT) and Y-intercept [ln(A)] give the $E_A$ and A terms as shown in Table 1. While β is known and fixed for the OTB testing heating rate conditions and the Kissinger decay function, Sihn et al. [11] describe how additional TGA data sets at different heating rates can be used to project variations in these parameters for any given heating rate β and any reaction model function.

# 4. RESULTS

## 4.1 Material Response Modeling

With the analytically difficult material properties determined (B' tables, pyrolysis gas enthalpy, and KMPs), data can be fed into the MR code of choice, ITRAC [14] in this case, and compared to the original in-situ temperature data acquired during OTB testing. Figure 10 below shows the one-dimensional simulated results from ITRAC of the MXB-360 glass/phenolic material compared against the OTB test data.

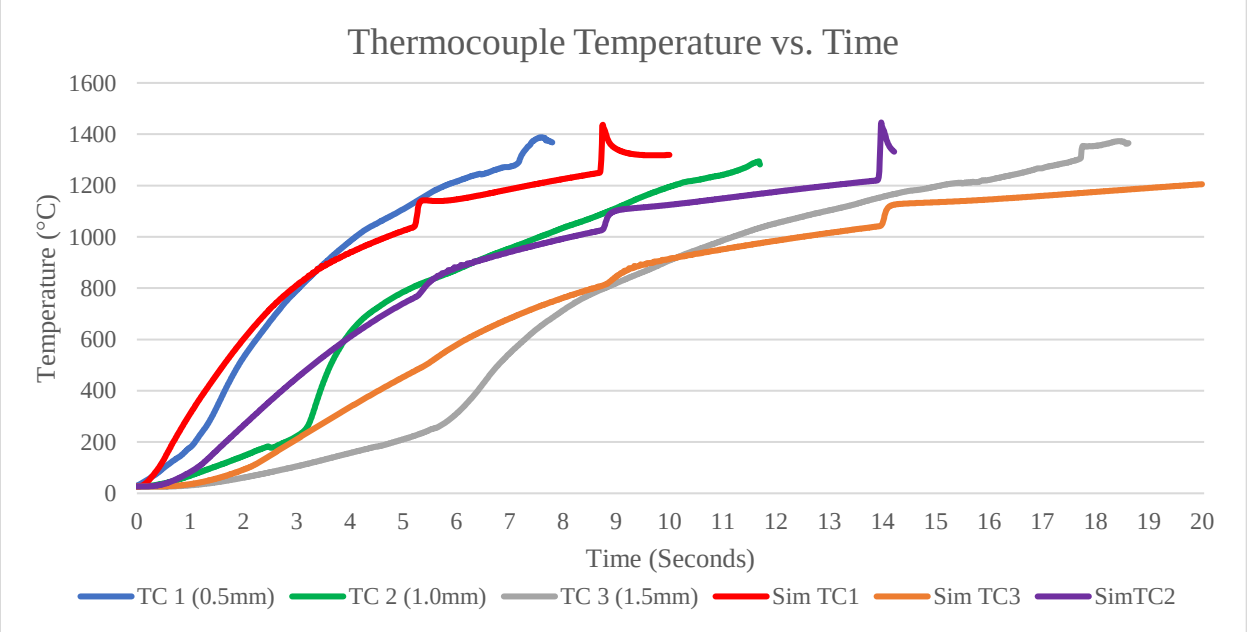


Figure 10. Temperature versus time graph for MXB-360 comparing OTB test data to simulated data in red from ITRAC. Note the temperature jumps on the simulated thermocouples: this is due to how ITRAC moves the ablation boundaries in steps.

While the simulation trends appropriately with respect to ablation behavior, the poor separation of pyrolysis reactions two and three during KMP determination results in differing heating rates, and slight insulation from the initial char layer results in an overstated initial heating rate. Gaussian separation programs may be utilized to predict curves that correspond to reactions two and three to separate them further and provide better estimations of the mass fraction they compose. Code limitations prevent matching the rapid heating of the TC junctions as they extend out of the char layer. In this instance, the trends appear generally similar and both sets of curves share two inflection points. Fine tuning of KMPs and material properties would help provide a closer fit, but the given values may be appropriate for some users.

Given reliable TGA data, poorly matched simulation data are often the result of operator error due to the number of steps involved in KMP development. There is additional opportunity for errors to occur when inputting results into a MR model, such as leaving placeholder tables in the input code or manual data entry mistakes. Temperature curves are good tools for diagnosing these issues; a mismatch in the number of inflection points in the curve points directly to issues with KMP values or the incorrect number of reactions occurring in the simulation, while large temperature spikes bring attention to heat capacitance, density, and other material property tables, especially if they occur at a material interface within the test model. Care should be taken to diagnose problems with all inputs prior to dismissing a model for design or testing purposes.

### 4.2 Determining Validation Criteria

Finding an endpoint for acceptably accurate KMPs and MR code output is important to marking the end of analysis. A perfect simulation of test or historical results is good to strive for but may not be feasible for a given working timeline, especially considering that design teams may require the MR code output to continue with their work or may only require a limited level of fidelity for a decision point.

Mass fraction remaining or mass loss tends to track experimental results more reliably than recession depth in general, as recession depth can be accelerated greatly due to factors, such as material fracturing, flaws in the production process, large pores in the heating zone, aerothermal channeling effects, and so on. Recession depth may not be useable for materials with significant swelling properties, such as engineering thermoplastics. Advection processes are not simple to control during test conditions, and average material thickness is simple to correlate to mass remaining, so mass fraction accuracy is an acceptable compromise unless working with a highly minimized safety factor.

In-depth temperature profile matching, as shown previously in Figure 10, can work well but is highly sensitive to sensor placement and to environmental effects. For example, a backside temperature sensor may show instantaneous cooling as the test model or torch are moved away from each other due to air flow, which may not be immediately obvious and may cause the analyst to dismiss the code output as improper when it is not. The simulated curves in Figure 10 demonstrate that the simulated ablation boundary is approximately 0.25 mm shallower than the OTB ablation boundary within the first 20 seconds, which may be within acceptable error for the purposes of considering the model to be validated for design or selection purposes.

## 5. SUMMARY

A rapid methodology for characterizing the ablation properties of materials was outlined in order to aid in reducing the cost and scheduling burden normally associated with flight testing materials or using hypersonic wind tunnels for TPS down selection. Data analysis was detailed for the use of TGA to determine reaction KMPs, EDX for elemental composition, and in-situ ablation sensing on an aerothermal

test bed for KMP validation. As KMPs are dependent on the user's choice of Kissinger, Friedman, or Ozawa reaction order functions, KMP validation is based on temperature curve trends compared against real world test data in order to determine their predictive capability. Both environmental composition and oxidative level are assumed to be fixed over time, so any changes would introduce significant error to MR modeling, requiring KMPs to be recalculated. Validation of a given MR model must consider the ability to match mass loss, surface temperature, backside temperature, and recession data when subjected to aerothermal testing using a variety of heat fluxes. Additional validations of the MR model are in progress.

# 6. REFERENCES


1. Starkey, R.P. and M.J. Lewis, *Critical Design Issues for Airbreathing Hypersonic Waverider Missiles.* Journal of Spacecraft and Rockets, 2001. **38**(4): p. 510-519.
2. Szczepanowska, H. and T.G. Mathia, *Space Heritage: The Apollo Heat Shield; Atmospheric Reentry Imprint on Materials' Surface.* MRS Proceedings, 2011. **1319**.
3. Suzuki, T., et al., *Postflight Thermal Protection System Analysis of Hayabusa Reentry Capsule.* Journal of Spacecraft and Rockets, 2014. **51**(1): p. 96-105.
4. Knight, D., et al., *Assessment of predictive capabilities for aerodynamic heating in hypersonic flow.* Progress in Aerospace Sciences, 2017. **90**: p. 39-53.
5. Paglia, L., et al., *Carbon-phenolic ablative materials for re-entry space vehicles: plasma wind tunnel test and finite element modeling.* Materials & Design, 2016. **90**: p. 1170-1180.
6. MacDonald, M.E., C.M. Jacobs, and C.O. Laux, *Interaction of Air Plasma With Ablating Heat Shield Material.* IEEE Transactions on Plasma Science, 2014. **42**(10): p. 2658-2659.
7. Natali, M., et al., *An in-situ ablation recession sensor for carbon/carbon ablatives based on commercial ultra-miniature thermocouples.* Sensors and Actuators B: Chemical, 2014. **196**: p. 46-56.
8. Koo, J.H., et al., *In Situ Ablation Recession and Thermal Sensor for Thermal Protection Systems.* Journal of Spacecraft and Rockets, 2018. **55**(4): p. 783-796.
9. Ewing, M.E. and B. Pincock, *Heat Transfer Modeling of a Charring Material Using Isoconversional Kinetics.* Heat Transfer Engineering, 2016. **38**(13): p. 1189-1197.
10. Ewing, M.E., T.S. Laker, and D.T. Walker, *Numerical Modeling of Ablation Heat Transfer.* Journal of Thermophysics and Heat Transfer, 2013. **27**(4): p. 615-632.
11. Sihn, S., et al., *Identifying unified kinetic model parameters for thermal decomposition of polymer matrix composites.* Journal of Composite Materials, 2018. **53**(20): p. 2875-2890.
12. Ozawa, T., *A New Method of Analysing Thermogravimetric Data.* Bulletin of the Chemical Society of Japan, 1965. **38**.
13. Yee, C., et al., *In Situ Ablation Recession Sensor for Ablative Materials Based on Ultraminiature Thermocouples.* Journal of Spacecraft and Rockets, 2014. **51**(6): p. 1789-1796.
14. Ewing, M.E. and D.A. Isaac, *Thermodynamic Property Calculations for Equilibrium Mixtures.* Journal of Thermophysics and Heat Transfer, 2018. **32**(1): p. 118-128.